

Electric Line Source Illumination of Lossless Left-Handed Cylinders - A Study of Near-Field and Far-Field Properties

Samel Arslanagić and Olav Breinbjerg

Ørsted•DTU, Electromagnetic Systems, Technical University of Denmark,

Building 348, Ørsted's Plads, DK-2800 Kgs. Lyngby, Denmark,

Tel: +45 4525 3800, Fax: +45 4593 1634,

E-mail: sar@oersted.dtu.dk, ob@oersted.dtu.dk

Abstract

We investigate the scattering of a left-handed circular cylinder illuminated by an electric line source. First, the analytical solution in terms of an eigenfunction series is derived. Second, this solution is used in numerical calculations to investigate the properties of the near-field, inside as well as outside the cylinder, and the far-field. This is done for different geometrical and electrical parameters. The radiation resistance and the directivity are calculated and the variation of these with different parameters is studied.

1 Introduction

Left-handed (LH) materials, which are the materials having a negative permittivity and permeability, have received much interest in recent years due to the several unfamiliar electromagnetic properties of these [1]. In particular, the lossless LH slab has been of significant interest due to its so-called “perfect lens” property [2], [3], but other configurations have been investigated as well [4], [5], [6]. Previous investigations on LH-cylinder configurations concerned evaluation of their scattering width under plane wave illumination [4], [5], and their cavity and waveguide properties [5].

In this work we investigate the scattering of a LH circular cylinder illuminated by an electric line source (ELS). First, the analytical solution in terms of an eigenfunction series is derived (Sec. 2). The solution is initially derived for the right-handed (RH) cylinder problem, which is characterized by both material parameters being positive, and subsequently the steps necessary to obtain the LH cylinder solution are outlined. Second, this solution is used in numerical calculations (Sec. 3) to investigate properties of the near-field, inside as well as outside the cylinder, and the far-field. This is done for different geometrical and electrical parameters such as cylinder radius, ELS position, cylinder permittivity and permeability. The radiation resistance and the directivity are calculated and the variation of these with different parameters is studied. Throughout the investigations the case of a RH cylinder is used as reference. The time factor $\exp(j\omega t)$, with ω being the angular frequency and t being the time, is assumed and suppressed.

2 Analytical Treatment of RH and LH Cylinders

The scattering configuration, consisting of a RH or LH cylinder illuminated by an ELS of a constant electric current I_e [A] placed parallel to the cylinder, is depicted in Figure 1.

The cylinder is located in the cylindrical coordinate system (ρ, ϕ, z) with the associated Cartesian coordinate system (x, y, z) as shown in the figure. It is of infinite extent in the z -direction, has a radius denoted by a , and is centered at the origin of the coordinate systems. The ambient medium is free space, with permittivity and permeability, respectively, $\epsilon_0 = 8.854 \cdot 10^{-12}$ [F/m] and $\mu_0 = 4\pi \cdot 10^{-7}$ [H/m]. The permittivity and the permeability of the cylinder are real scalars denoted by $\epsilon_c = \epsilon_r \epsilon_0$ and $\mu_c = \mu_r \mu_0$, respectively, where ϵ_r and μ_r , respectively, are its relative permittivity and permeability. The wavenumber inside the cylinder is denoted by $k_c = k_0 \sqrt{\epsilon_r \mu_r}$, where $k_0 = \omega \sqrt{\epsilon_0 \mu_0} = 2\pi/\lambda_0$ is the free-space wavenumber and λ_0 is the free-space wavelength, while the intrinsic

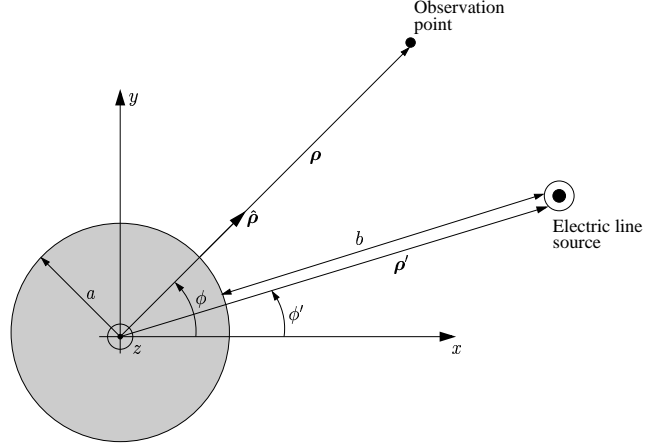


Figure 1: Scattering configuration under consideration: a RH or LH cylinder illuminated by an ELS located in free space.

impedance of the cylinder is $\eta_c = \eta_0 \sqrt{\mu_r/\epsilon_r}$, where $\eta_0 = \sqrt{\mu_0/\epsilon_0}$ is the free-space intrinsic impedance. When the cylinder is RH, $\epsilon_r > 0$, $\mu_r > 0$, and $k_c > 0$, $\eta_c > 0$. When the cylinder is LH, $\epsilon_r < 0$, $\mu_r < 0$, and we choose $k_c < 0$ and $\eta_c > 0$. As shown in [7] either a positive or a negative wavenumber can be chosen, since the results obtained with either choice of sign agree. However, the present choice is convenient since the solution to the RH cylinder problem then applies directly for the LH cylinder problem simply by using negative values for ϵ_r , μ_r , and k_c .

The position vector of a given observation point is $\boldsymbol{\rho}$ (with the corresponding unit vector $\hat{\boldsymbol{\rho}}$), and its coordinates are (ρ, ϕ) , while the position vector of the ELS is $\boldsymbol{\rho}'$, and its coordinates are (ρ', ϕ') . The distance between the ELS and the cylinder surface is denoted by b .

In the absence of the cylinder the field due to the ELS is [8, Ch. 11]

$$\mathbf{E}^i(\rho, \phi) = -\hat{\mathbf{z}} I_e \frac{\omega \mu_0}{4} H_0^{(2)}(k_0 |\boldsymbol{\rho} - \boldsymbol{\rho}'|) = -\hat{\mathbf{z}} I_e \frac{\omega \mu_0}{4} \begin{cases} \sum_{n=-\infty}^{\infty} J_n(k_0 \rho) H_n^{(2)}(k_0 \rho') e^{jn(\phi - \phi')} & \text{for } \rho \leq \rho', \\ \sum_{n=-\infty}^{\infty} J_n(k_0 \rho') H_n^{(2)}(k_0 \rho) e^{jn(\phi - \phi')} & \text{for } \rho \geq \rho', \end{cases} \quad (1)$$

with $\rho = |\boldsymbol{\rho}|$, and $\rho' = |\boldsymbol{\rho}'|$, see Figure 1. The function $J_n(\cdot)$ is the Bessel function of order n , while $H_n^{(2)}(\cdot)$ is the Hankel function of the second kind and order n . $\hat{\mathbf{z}}$ is the unit vector pointing in the z -direction. In similitude with the expansion for \mathbf{E}^i , the scattered and the transmitted electric fields, denoted by \mathbf{E}^s and \mathbf{E}^t , respectively, are expanded as

$$\mathbf{E}^s(\rho, \phi) = -\hat{\mathbf{z}} I_e \frac{\omega \mu_0}{4} \sum_{n=-\infty}^{\infty} a_n H_n^{(2)}(k_0 \rho) e^{jn(\phi - \phi')} \quad \text{for } \rho \geq a, \quad (2)$$

$$\mathbf{E}^t(\rho, \phi) = -\hat{\mathbf{z}} I_e \frac{\omega \mu_c}{4} \sum_{n=-\infty}^{\infty} b_n J_n(k_c \rho) e^{jn(\phi - \phi')} \quad \text{for } \rho \leq a, \quad (3)$$

where a_n and b_n are the unknown expansion coefficients. The incident, scattered, and transmitted magnetic fields, respectively, are readily obtained from the Faraday's induction law. The continuity conditions are then applied at the cylinder surface in order to determine a_n and b_n , and the final result is

$$a_n = H_n^{(2)}(k_0 \rho') \frac{J_n'(k_0 a) J_n(k_c a) - (\eta_0/\eta_c) J_n(k_0 a) J_n'(k_c a)}{(\eta_0/\eta_c) J_n'(k_c a) H_n^{(2)}(k_0 a) - J_n(k_c a) H_n^{(2)'}(k_0 a)}, \quad (4)$$

$$b_n = \frac{\mu_0}{\mu_c} H_n^{(2)}(k_0 \rho') \frac{J_n(k_0 a) H_n^{(2)'}(k_0 a) - J_n'(k_0 a) H_n^{(2)}(k_0 a)}{J_n(k_c a) H_n^{(2)'}(k_0 a) - (\eta_0/\eta_c) J_n'(k_c a) H_n^{(2)}(k_0 a)}. \quad (5)$$

Note that all derivatives in the above equations are to be taken with respect to the function's argument.

The solution (1)-(5) applies to a RH cylinder if $\epsilon_r > 0$, $\mu_r > 0$, $k_c > 0$, and $\eta_c > 0$, and to a LH cylinder if $\epsilon_r < 0$, $\mu_r < 0$, $k_c < 0$, and $\eta_c > 0$.

3 Numerical Treatment of RH and LH Cylinders

3.1 Near-Field Properties

The near-field, denoted by $\mathbf{E}(\rho, \phi)$, is calculated inside as well as outside the cylinder ¹. More specifically, the quantity $20 \log_{10} |\mathbf{E}(\rho, \phi)| / 1 \text{ [V/m]} \text{ [dB]}$ is shown in a circular region of radius $3\rho'$ centered at the cylinder axis (z -axis), see Figure 1. To facilitate comparison of the results, the dynamic range is kept constant throughout the forthcoming figures.

The effect of the LH cylinder is particularly notable in the case of a “ $1\epsilon_0 1\mu_0$ ” cylinder. A few examples of such results are shown in Figure 2, which depicts the near-field distributions for the cylinders having radii $2\lambda_0$ and $4\lambda_0$. In both cases the ELS is located at $b = 1\lambda_0$.

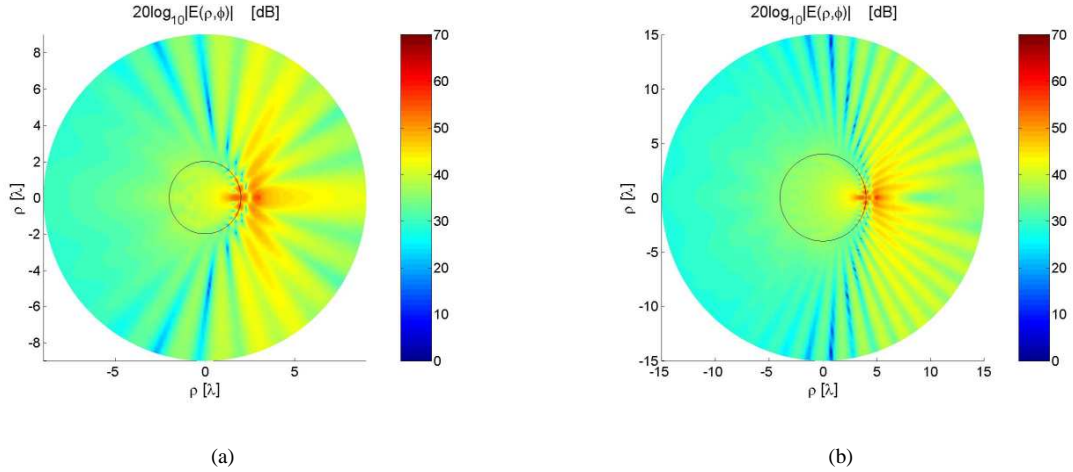


Figure 2: Electric field distribution for “ $1\epsilon_0 1\mu_0$ ” LH cylinders having radii $a = 2\lambda_0$ (a) and $a = 4\lambda_0$ (b). The ELS is at $b = 1\lambda_0$.

Since the corresponding RH cylinders would simply be those of free space, and the resulting field thus omnidirectional, it is obvious that the considered LH cylinders have a significant effect by creating a field pattern with several lobes and a shadow region. It is observed that the variation of the field pattern is more pronounced for the cylinder of the larger radius. In addition, in both cases, there appears to be a formation of a point inside the cylinders at which the field takes on very high values. This formation is more clear for the cylinder of the larger radius, and suggests that some focusing of the ELS field is taking place inside the cylinders. However, contrary to the well-known case of the lossless LH slab of the same material parameters, see e.g., [1] and [2], no high field values are observed in the region to the left of the cylinder along the negative x -axis. Moreover, the point inside the cylinders at which the field attains a high value does not represent an exact image of the ELS since the cylinder surface is curved and its aperture is finite. In addition to the high field value inside the cylinders, the field also attains rather high values along the part of the cylinder surface which is close to the ELS.

Figure 3 shows the field for “ $2\epsilon_0 1\mu_0$ ” RH (a) and LH (b) cylinders of radius $a = 2\lambda_0$, and the ELS located at $b = 1\lambda_0$. For RH cylinders a clear beam formation along the negative x -axis is observed. Some field variation is observed in the half-space in which the ELS is located, and no shadow region is formed. Regarding the LH cylinder

¹Two remarks are in order. First, it is noted that in all of the forthcoming calculations the ELS is at a distance b from the cylinder along the positive x -axis, see Figure 1. Second, for easy reference, a cylinder having the material parameters $(\epsilon_c, \mu_c) = (\epsilon_r \epsilon_0, \mu_r \mu_0)$, with ϵ_r and μ_r being the relative permittivity and permeability, respectively, is referred to as a “ $\epsilon_r \epsilon_0 \mu_r \mu_0$ ” RH cylinder for $\epsilon_r > 0$, $\mu_r > 0$, and as a “ $|\epsilon_r| \epsilon_0 |\mu_r| \mu_0$ ” LH cylinder for $\epsilon_r < 0$, $\mu_r < 0$.

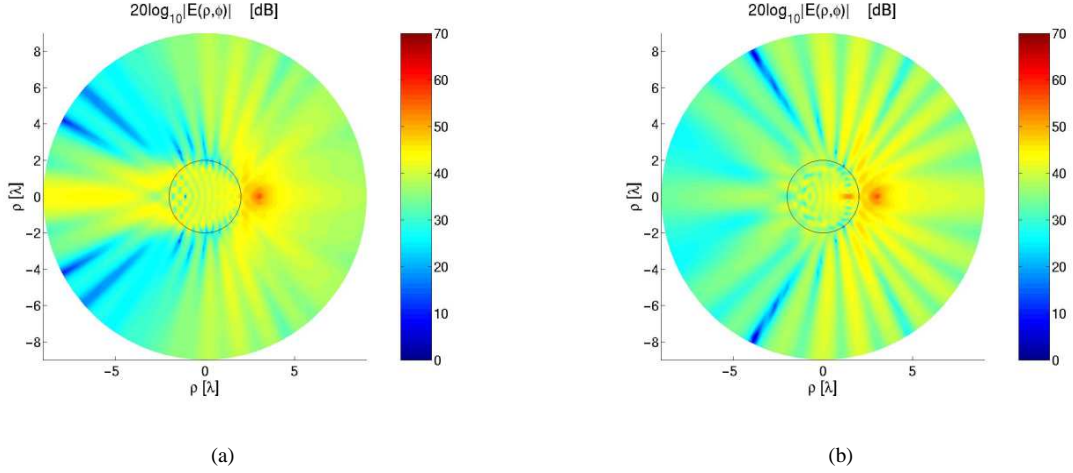


Figure 3: Electric field distribution for “ $2\epsilon_0 1\mu_0$ ” RH (a) and LH (b) cylinders having radius $a = 2\lambda_0$. The ELS is at $b = 1\lambda_0$.

configuration, the field pattern exhibits rather large variations. In addition, the field outside the LH cylinder is mainly confined to the half-space in which the ELS is located. Furthermore, the field variation is more pronounced for the LH than for the RH cylinders in the sense that much deeper zeros are observed in the pattern. Regarding the field transmitted into the LH cylinder, a clear formation of a high field value is observed, this being more clear than with the previously shown results for “ $1\epsilon_0 1\mu_0$ ” cylinders, again suggesting that some focusing of the ELS field is taking place.

3.2 Far-Field Properties

First, the two-dimensional directivity, henceforth referred to as the directivity, given by

$$D(\phi) = \frac{2\pi |\mathbf{E}_f^{tot}(\phi)|^2}{\int_{\phi=0}^{2\pi} |\mathbf{E}_f^{tot}(\phi)|^2 d\phi} = \frac{2\pi |\mathbf{E}_f^i(\phi) + \mathbf{E}_f^s(\phi)|^2}{\int_{\phi=0}^{2\pi} |\mathbf{E}_f^i(\phi) + \mathbf{E}_f^s(\phi)|^2 d\phi}, \quad (6)$$

is investigated. In (6) \mathbf{E}_f^{tot} designates the total far-field pattern which is the sum of the incident, \mathbf{E}_f^i , and the scattered, \mathbf{E}_f^s , far-field patterns. These are easily obtained from (1) (the expression for $\rho \geq \rho'$) and (2), respectively, through a large argument expansion of the involved Hankel function and subsequent normalization with $\exp(-jk\rho)/\sqrt{\rho}$. Second, the radiation resistance, R_{rad}^{tot} , of the system comprising a given cylinder and the ELS is calculated and subsequently normalized to the radiation resistance, R_{rad}^i , due to the ELS alone. The so-obtained quantity is denoted by R_{rad}^{norm} and is given by

$$R_{rad}^{norm} = \frac{R_{rad}^{tot}}{R_{rad}^i} = \frac{P_{rad}^{tot}}{P_{rad}^i}, \quad (7)$$

with P_{rad}^{tot} denoting the power radiated by the system, and P_{rad}^i denoting the power radiated by the ELS alone, and

$$P_{rad}^{tot} = \frac{1}{2\eta_0} \int_{\phi=0}^{2\pi} |\mathbf{E}_f^{tot}(\phi)|^2 d\phi, \quad \text{and} \quad P_{rad}^i = \frac{1}{2\eta_0} \int_{\phi=0}^{2\pi} |\mathbf{E}_f^i(\phi)|^2 d\phi. \quad (8)$$

3.2.1 Directivity

Figure 4a) and b) shows the directivity for the “ $1\epsilon_0 1\mu_0$ ” LH cylinder configuration of which the near fields were depicted in Figure 2. The directivity for the corresponding RH cylinder is shown as well, and is, of course, uniformly distributed. The LH cylinders do not exhibit any lobe formation, and the pattern contains a number of ripples, this being more pronounced for the cylinder of the larger radius. These observations are in accordance

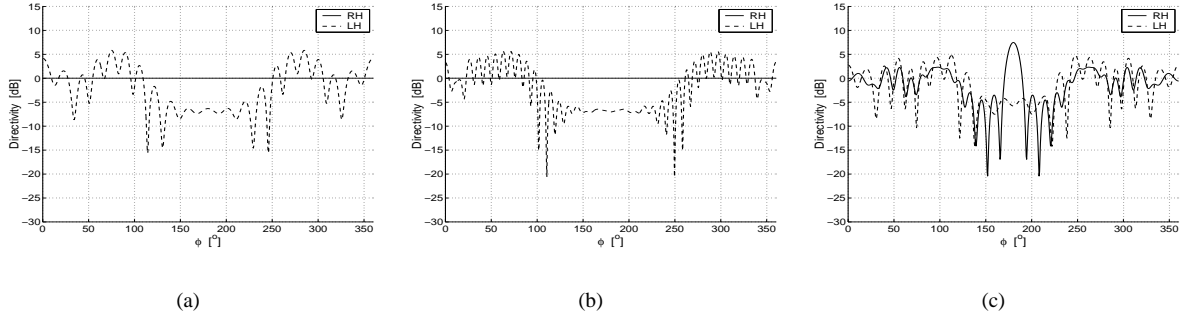


Figure 4: Directivity for “ $1\epsilon_0 1\mu_0$ ” RH and LH cylinders having radii $a = 2\lambda_0$ (a) and $a = 4\lambda_0$ (b). (c) Directivity for “ $2\epsilon_0 1\mu_0$ ” RH and LH cylinders having radius $a = 2\lambda_0$. In all cases, the ELS is at $b = 1\lambda_0$ to the right of the cylinder.

with the near-field results shown in Figure 2. The formation of a shadow region is obvious in both cases since the directivity attains much lower values for $\phi \in [125^\circ, 225^\circ]$ than for $\phi \in [0^\circ, 125^\circ[\cup]225^\circ, 360^\circ[$.

Similar observations apply for cylinders of other material parameters. Figure 4c) shows the directivity for “ $2\epsilon_0 1\mu_0$ ” RH and LH cylinders of which the near fields were shown in Figure 3. A clear lobe formation is observed for the RH cylinder in the angular region close to the $\phi = 180^\circ$ direction. As the observation point is moved away from this direction, the pattern becomes ripple-like. The LH cylinder directivity is observed to contain no distinct lobe, but instead a number of ripples in the pattern. The shadow region around $\phi = 180^\circ$ is easily identified.

3.2.2 Radiation Resistance

In Figure 5 the results for R_{rad}^{norm} are shown for “ $1\epsilon_0 1\mu_0$ ” and “ $2\epsilon_0 1\mu_0$ ” RH and LH cylinders as function of cylinder radius a for different locations of the ELS (those radii for which R_{rad}^{norm} was calculated are indicated by the various markers in the figure).

There is, of course, no variation for the “ $1\epsilon_0 1\mu_0$ ” RH cylinders, see Figure 5a), while the case of the “ $1\epsilon_0 1\mu_0$ ” LH cylinders is seen to exhibit some variation of R_{rad}^{norm} as a changes. For the “ $2\epsilon_0 1\mu_0$ ” cylinder, see Figure 5b), R_{rad}^{norm} is seen to be slightly varying with a . However, the variation is somewhat more pronounced for LH than for RH cylinders.

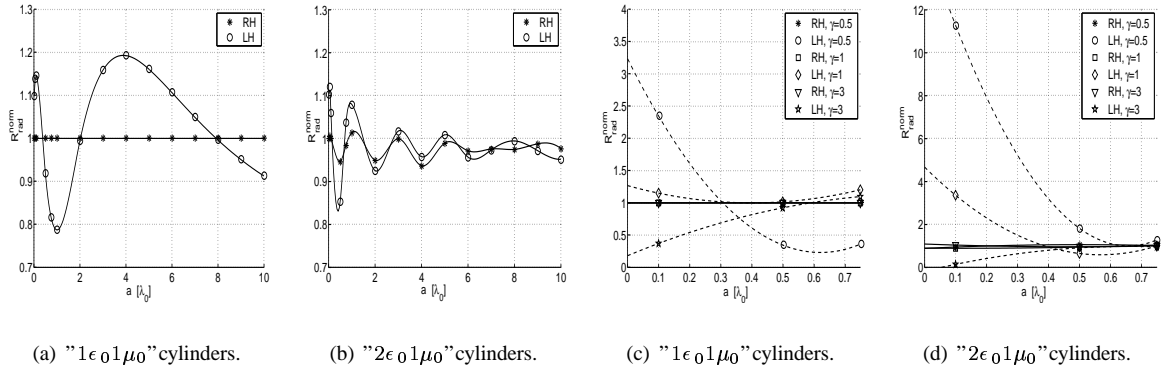


Figure 5: Variation of the normalized radiation resistance as function of the cylinder radius, a , for RH and LH cylinders of various material parameters. The ELS is at $b = 1\lambda_0$ [figures (a) and (b)] and $b = \gamma a \lambda_0$, $\gamma = [0.5, 1, 3]$ [figures (c) and (d)].

The observed variation in R_{rad}^{norm} is particularly significant in the case of LH cylinders having a fairly small radius and the ELS placed close to it, see Figure 5c) and d), for $\gamma = 0.5$. While the results for “ $1\epsilon_0 1\mu_0$ ” RH cylinders are as expected, the “ $1\epsilon_0 1\mu_0$ ” LH cylinders exhibit rather pronounced variation of R_{rad}^{norm} with a . The “ $2\epsilon_0 1\mu_0$ ” RH cylinders do not show nearly as large variation as the corresponding LH cylinders. It is noted that in the

present case the results are recorded for $a = [0.1, 0.5, 0.75] [\lambda_0]$ only, since numerical calculations showed rather moderate variation of R_{rad}^{norm} for larger a for both RH and LH cylinders.

4 Conclusions

We have investigated the scattering of a LH circular cylinder illuminated by an ELS. The analytical solution was first derived for the case of RH cylinders and second, the steps necessary to treat LH cylinders were outlined. Subsequently, numerical calculations of the near-field, inside as well as outside the cylinder, and the far-field, in terms of the directivity and the radiation resistance, were performed for different geometrical and electrical parameters such as cylinder radius, ELS position, cylinder permittivity and permeability.

It was shown that the effect of the LH cylinder is most notable in the case of " $1\epsilon_0 1\mu_0$ " cylinders for which the near-field results revealed a formation of a field pattern with several lobes and a shadow region. This was found to be in sharp contrast to the corresponding RH cylinders for which the field is, of course, omnidirectional. Moreover, a high field value formation was observed at a point inside the LH cylinders suggesting that some focusing of the ELS field is taking place. Similar features were observed for the " $2\epsilon_0 1\mu_0$ " LH cylinder, but the high field value at a point inside the cylinder is more clear. No distinct main lobe could be observed in the pattern for the " $2\epsilon_0 1\mu_0$ " LH cylinder, while the corresponding RH cylinder was found to be rather directive as it exhibited a clear main lobe. It was furthermore shown that the near-field results are well in agreement with the directivity which is rather ripple-like and without a distinct main lobe for the LH cylinders. In contrast to this, in the case of the " $2\epsilon_0 1\mu_0$ " RH cylinder, the directivity was observed to possess a clear main lobe, while, of course, being uniform for the " $1\epsilon_0 1\mu_0$ " RH cylinders. The radiation resistance varied more for LH cylinders than for RH cylinders as function of their radius. This was in particular the case for " $1\epsilon_0 1\mu_0$ " and " $2\epsilon_0 1\mu_0$ " LH cylinders (" $1\epsilon_0 1\mu_0$ " RH cylinders exhibited, of course, no variation) of small radii and the ELS placed close to their surface.

References

- [1] V. G. Veselago, "The electrodynamics of substances with simultaneously negative values of ϵ and μ ," *Sov. Phys. Usp.*, Vol. 10, No. 4, pp. 509-514, Jan.-Feb. 1968.
- [2] J.B. Pendry, "Negative refraction makes a perfect lens," *Phys. Rev. Lett.*, Vol. 85, No. 18, pp. 3966-3969, Oct. 2000.
- [3] N. Garcia, and M. Nieto-Vesperinas, "Left-handed materials do not make a perfect lens," *Phys. Rev. Lett.*, Vol. 88, No. 20, pp. 4031-4034, May 2002.
- [4] V. Kuzmiak, and A. A. Maradudin, "Scattering properties of a cylinder fabricated from a left-handed material," *Phys. Rev. B.*, Vol. 66, No. 4, pp. 1161-1167, July 2002.
- [5] A. Alù, and N. Engheta, "Resonances in sub-wavelength cylindrical structures made of pairs of double-negative and double-positive or ϵ -negative and μ -negative coaxial shells," *Dig. of ICEAA'03*, pp. 435-438, Turin, Italy, Sept. 8-12, 2003.
- [6] R. Ruppin, "Extinction properties of a sphere with negative permittivity and permeability," *Solid State Commun.*, Vol. 116, pp. 411-415, Aug. 2000.
- [7] S. Arslanagic, and O. Breinbjerg, "A note on the sign of some important parameters for left-handed materials," Internal Report, IR 781, Ørsted•DTU, Electromagnetic Systems, Technical University of Denmark, July 2004.
- [8] C. A. Balanis, "Advanced engineering electromagnetics", *New York: John Wiley & Sons, Inc.*, 1989.

Olav Breinbjerg was born in Silkeborg, Denmark in 1961. He received the M.S.E.E. and Ph.D. degrees from the Technical University of Denmark (DTU), Lyngby, Denmark, in 1987 and 1992, respectively. Since 1991 he has been on the faculty of Ørsted- DTU, Electromagnetic Systems, DTU, where he is now an Associate Professor and Head of the Antenna and Electromagnetics Group comprising also the DTU-ESA Spherical Near-Field Antenna Test Facility.

He was a visiting Research Scientist at the Rome Laboratory, Hanscom Air Force Base, MA in the fall of 1988 and a Fulbright Scholar at the University of Texas, Austin, TX in the spring of 1995. His research interests include electromagnetic field theory, asymptotic and computational electromagnetics, antennas, and scattering. Several contributions have been made to high frequency asymptotic techniques such as Physical Optics (PO), Physical Theory Diffraction (PTD) and Geometrical Theory Diffraction (GTD). He was the Representative of Management Comitee of COST-260 Action on Smart Antennas and COST-284 Action on Innoative Antennas. He is also a member of Executive Board of EU 6th Framework Programme on Antenna Center of Excellence.

Dr. Breinberg received the 2001 AEG Electron Foundation Award and 2003 DTU Student Union's Teacher of the Year Award.

Olav Breinbjerg Silkeborg Danimarka'da 1961 yılında doğmuştur. Yüksek Lisans ve Doktora derecelerini Danimarka Teknik Üniversitesi (DTU) Elektrik Mühendisliği Bölümünden sırasıyla 1987 ve 1992 yıllarında almıştır. 1991 yılından bu yana DTU'dedir. Şu anda aynı üniversitede Doçent olarak Anten ve Elektromanyetik Grubunun başkanlığı yürütmekte ve DTU-ESA Küresel Yakın Alan Anten Test Tesisinde çalışmaktadır.

1988 sonbaharında Rome Labaratuvarında araştırmacı olarak ve de 1995 baharında Fullbright bursu ile Texas Üniversitesinde bulunmuştur. Araştırmaları elektromanyetik alan teorisi, asimtotik ve hesaplamasal elektromanyetik, antenler, ve saçınım üzerinedir. Fiziksel Optik (PO), Kırınımın Fiziksel Teorisi (PTD) ve Kırınımın Geometrik Teorisi (GTD) gibi yüksek frekans asimtotik tekniklere çeşitli katkıları bulunmaktadır.

Dr. Breinbjerg COST-286 Action on Smart Antennas ve COST-284 Action on Innovative Antennas yönetim kurulu temsilciliği yapmıştır. Ayrıca 6. Avrupa Framework Programme on Antenna Center of Excellence üst yönetim kurulu üyesidir. 2001 yılı AEG Elektron Vakfı Ödülü ve de 2003 yılı DTU Öğrenci Birliği Yılın Öğretmeni Ödülünü almıştır.